IMAV2017-7
https://www.imavs.org/pdf/imav.2017.7

Aeroacoustics Investigation on Nano Coaxial Rotor in Hover

Zhen Liu1,* Chen Bu2, Xiangxu Kong3, and Dong Yang3
State Key Laboratory for Strength and Vibration of Mechanical Structures, school of Aerospace Xi'an Jiaotong University, Xi'an, China

ABSTRACT

Aeroacoustics of nano rotor has an impact on the stability and reliability of nano air vehicle. The interference between rotors on aeroacoustics was investigated for nano coaxial counter-rotating rotor. The aerodynamic model of upper rotor of nano rotor was firstly established with sliding mesh technique and multi-blocks method. The unsteady flow field of upper rotor was then studied with LES method and the pressure, the velocity and the vorticity distribution were analyzed. On the basis of the analysis of flow field, the FW-H method was used to study the aeroacoustics of upper rotor. The total sound pressure level and the frequency noise spectrum of the upper rotor were monitored. In order to verify the results of simulation, the test bench for measuring the aeronautics of upper rotor was established. The variation of sound pressure level was measured. The results between the simulation and experiment were compared. It was found that the sound pressure level of monitor point which is near the vortex is high. In the frequency noise spectrum, there is an integer in multiple of the rotation frequency and fundamental frequency, and the peak value decreases with the increase of frequency. The experimental aeroacoustics results match well with that of the computational results so that the computational method is validated. The aeroacoustics of nano coaxial rotor was then studied numerically. When comparing with upper rotor, it was found that the SPL of nano coaxial rotor increased. Flow field analysis showed that the shedding vortices of upper rotor interact the lower rotor resulting the blade-vortex interaction. It is evident that the aeroacoustics was enhanced by the interference of upper rotor and lower rotor.

1 INTRODUCTION

Nano air vehicle (NAV) [1] proposed by Defense Advanced Research Projects Agency (DARPA) in 2005 have attracted more attention in recent years. It is required to fulfill missions in complex and cluttered environments with a hovering capacity that allows for the timely collection of comprehensive intelligence information [2, 3, 4]. Rotary-wing NAV is one kind of NAV driving with rotors with dimension less than 7.5cm in length and payloads of up to 2g and is capable of hovering and flying at a low speed. The nano rotor mainly generates the low-frequency noise due to its low rotational velocity, which increases the difficulty to fly undetected in narrow space. And the NAV structure vibrates with the aeroacoutic load, which might induce the fatigue damage of the structure so that the reliability of the NAV is reduced [5]. For nano coaxial rotor, it generates more noise because of the strong interaction between the upper rotor and the lower rotor. Therefore, it is necessary to investigate the aeroacoustic characteristics of nano coaxial rotor so as to improve the reliability and performance of NAV.

Analytical method and experimental method are usually two methods widely used to study the aeroacoustics of rotor. Kirchhoff method [6] and Ffowcs-Williams/Hawking equation (FW-H) method [7, 8] are two main analytical methods. Kirchhoff meothod can calculate effectivley the nonlinear acoustics including the quadrapole source and is an important method to calculate the high velocity impulse noise of helicopter rotor. However, this method only gives a solution of a total sound pressure but do not isolate the source related to blade thickness, the source linked to the aerodynamic loading and the quadrapole source so that the physical sense of acoustics is not clear. FW-H method usually takes into account a monopole item and a dipole item. But it is difficult to solve the quadrapole item. So it is suitable for the calculation of the source related to blade thickness and the source linked to the aerodynamic loading. FW-H is an appropriate method for the research on the aeroacoustic characteristics if there is no supersonic or transonic phenomenon. As nano coaxial rotor is small and rotates at a low velocity, FW-H method is applicable for nano rotor. In recent years, enormous amount of rotary-wing MAV were developed with the development of the micro air vehicle. Lots of researches were carried out on aeroacoustics of micro rotor. Giorgia etc. [9] applied FW-H method to study the aeroacoutic characteristics of a small propeller with a diameter of 60 cm. Marino [10] also used FW-H method to predict the noise of a propeller of an UAV. However, the aeronautic characteristics of small coaxial rotor are scarcely studied. The influence of rotor interference on aeroacoustics is not taken into account. Some research

*Email address(es): contact_liuz@mail.xjtu.edu.cn

work on full-scalle counter-rotating rotor was carried out. Yi etc. [11] developed a time-spectral RANS method to study the counter-rotating open rotor. The aeroacoustics analysis is carried out using the FW-H equations on the permeable integral surface. Housman etc. [12] used a coupled computational fluid dynamics and computational aeroacoustics numerical approach to study the aeroacoutic characteristics of a contra-rotating open rotor noise. Three-dimensional time-accurate hybrid Reynolds Averaged Navier-Stokes/Large Eddy Simulation (RANS/LES) CFD simulations are performed in the inertial frame. The aeroacoustic analysis is based on a permeable surface FW-H approach evaluated in the frequency domain. However, the inference between upper rotor and lower rotor was not studied. Despite of the fact that the full-scale rotor operates at a high Reynolds number and rotates at a high speed, the research approach can also be taken as a reference to study the nano coaxial rotor. Aeroacoustics experiments can be carried out in an anechoic room or in an open space. The experiment in the anechoic room has the advantage of low environment noise. But it is required that the room size is far larger than the rotor diameter to avoid the circumfluence due to the rotor wake. The experiment in an open space can alleviate the interference but the background noise is large. Giorgia etc. [9] and Marino [10] performed the aeroacoutics experiments of a small propeller in an anechoic room. In our research, an open space with a low-speed wind speed was chosen to carry out the experiment.

In this paper, a three-dimensional time-accurate Large Eddy Simulation (LES) CFD method coupling with FW-H method was used to study the aeroacoutics characteristics of nano coaxial rotor. The pressure and viscous force was taken as the input parameters for FW-H equations. And the quadrapole item was ignored when solving the FW-H equation. And the aeroacoustics experiments for single rotor were carried out to validate the approach. Then the influence of the interference between upper rotor and lower rotor was studied numerically.

2 Methodology and Experimental Setup

2.1 FW-H Equation

Aeroacoustics originates in the Lighthill formula established by Lighthill in 1952. But the most common method for the analysis of aeroacoutics for moving body is the FW-H equations developed by Ffowcs-Williams and Hawking in 1969 [7].

$$\begin{aligned}\frac{1}{c_0^2}\frac{\partial^2}{\partial t^2}\left[pH(f)\right] =& \frac{\partial}{\partial t}\left[\rho_0 V_i \frac{\partial f}{\partial x_i}\delta(f)\right] \\ &- \frac{\partial}{\partial x_i}\left[p_{ij}\frac{\partial f}{\partial x_j}\delta(f)\right] \\ &+ \frac{\partial^2}{\partial x_i \partial x_j}\left[T_{ij}H(f)\right]\end{aligned} \tag{1}$$

In this equation, the impact of the moving body and its boundary layer on the fluid is considered. The first item in the right side of the equation is a surface sound source decided by $\delta(f)$ function on the body surface which is called monopole source or the source related to body thickness. The second item in the right side of the equation is also a surface sound source decided by $\delta(f)$ function on the body surface. But it is a dipole source or a source linked to the aerodynamic loading. The third item is a volume sound source decided by $H(f)$ function distributed outside of the body. It is a quadrapole source which is related to the nonlinear flow. Monopole acoustic source and dipole acoustic source belong to the surface source which predominates in the total aeroacoustics. The quadrapole shall be calculated by integrating the whole flow field which is very difficult. Since the nano coaxial rotor rotates at a very low speed, the aeroacoustic surface source can only be considered.

2.2 Experimental Setup

The purpose of the experiment is to validate the computational method. The experimental setup consists of a rotor, a motor, a speed controller, a DC power, a BK acoustics measurement system and supports. An experimental setup is shown in Figure 1. The upper rotor of the coaxial rotor is tested. A micro brushless rotor with diameter of 13mm and weighted 2.3g was used to drive the rotor. A DC power is used to supply the energy. And the BK acoustics measurement system was used to measure the noise. A pair of nano

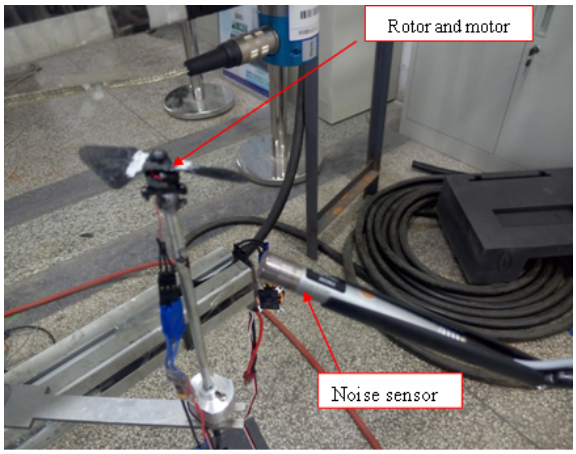

Figure 1: Aeroacoustics test bench for single rotor.

counter-rotating rotors with diameters of 7.5 cm was studied. The upper rotor has a mean chord of 0.33R and a mean twist angle of 17.21° , and the lower rotor has a mean chord of 0.31R and a mean twisted angle of 17.67° as illustrated in Figure **??**. The twist angle and the chord distribution were optimized to ensure the maximum FM at the working RPM during design. Conventional method is not applicable for the improvement of FM. The blade airfoil has a 2% constant thickness with a 5% camber circular arc.

IMAV2017-7
https://www.imavs.org/pdf/imav.2017.7

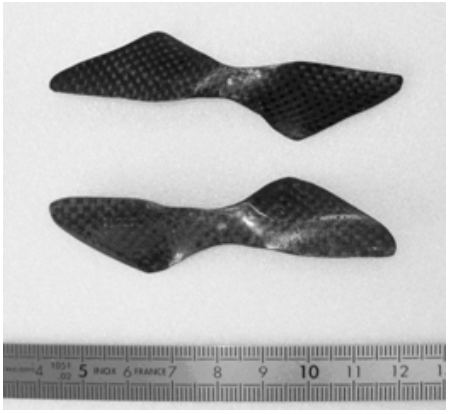

Figure 2: Nano coaxial rotor.

3 Results and discussion

3.1 Aeroacoustics Characteristics of Upper Rotor

Prior to the computation, the meshes of the upper rotor were generated. The multi-block structured mesh was generated. The boundary of the background mesh was formed by a 25.5R-high cylinder with top and bottom radii of 12R and 16R, respectively. In order to calculate the flow field precisely, the boundary method was generated and the thickness of the first layers satisfied with the Yplus in the order of 1. The total number of grid is about 10million.The sliding mesh method was used to describe the motion of the rotor and a three-dimensional time-accurate Large Eddy Simulation (LES) CFD method coupling with FW-H method was used to predict the noise of the upper rotor rotating at a velocity of 6500RPM in static condition. A commercial solver FLUENT was used in this research. The simulations were carried out on the upper rotor at a tip Mach of 0.075. The rotor rotated 1 deg at each physical time step. Rotors rotated more than 10 cycles. The computations were performed on an HP station with 40 Xeon 6290 CPU with 64 GB memory.

Figure 3 shows the vortex contour at the different stations along the blade. According to the theory of vortex and sound, the generation and shedding of the vortices induce pressure fluctuation resulting in the noise. It is found from the figures that trailing edge vortex generates and sheds from the blade. The separation of the boundary layer near the trailing edge induces a large vortex and the vortex sheds due to the instability of the flow. From the blade tip to the blade root, the flow field becomes more complicated and the vorticity magnitude increases. With the analysis of the flow field, the noise monitors were set according to the shedding of the vortex. The acoustics characteristics of the upper rotor were analyzed with FW-H equation method based on the transient analysis of the flow field. From the 4(a), three types of monitor points are presented in order to show the total sound pressure level in the wake. The first type of monitor points are the points located on the centerline of the rotor. The distance of the monitor

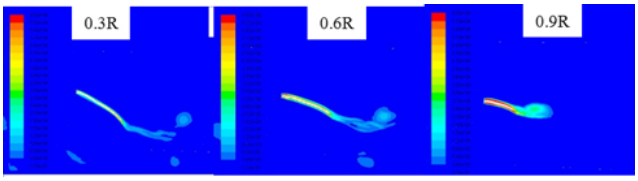

Figure 3: Vorticity contour at different blade station.

point to rotor disk is 3.5 mm, and the distance increases with a increment of 3.5 mm for the following monitor points. The second type of monitor points located in the lateral line of rotor. The first six points has the same vertical distance as the monitor points on the centerline, but the distance in the horizontal direction also increases with an increment of 2 mm. The last three points has the same horizontal distance. The third type of monitor points are generated to capture the tip vortex and locate at the horizontal distance of 0.85 radius of the rotor. Figure 4(b) shows the total sound pressure level at different monitor points. It is found that the OASPL of the monitor points at the blade tip is the highest. The OASPL along the centerline is the lowest. For the first type and the second type of monitor points, the OASPL increases with the distance at the beginning but then decreases with the distance. The OASPL of the monitor points at the blade tip decreases with the distance monotonously. The blade tip vortex, which is one of the main noise source, are very strong at the tip so that the OASPL of the monitor points at the blade tip is high. It is also showed that the OASPL increases from the blade root to the blade tip. Figure 5 shows the total sound pressure level at different monitor points at different radius and angle in the vertical plane. In the rotor disk plane, the OASPL is 95.7dB at 1.2R but it is 81.4R at 1.8R. In the vertical plane, it is found that the OASPL is 85.9dB at the angle of 30 ° but it is 76.5dB at the angle of 60 °. Results illustrate that the OASPL decreases as the radius and the angle increase.

The frequency-analysis could show more information at each monitor points. Therefore, three monitor pints which have the maximum OASPL each type of monitor points were selected to analyze in frequency domain. As the rotational velocity of nano rotor is not too high and the frequency of the rotational noise is in low-frequency range, the cut-off frequency is 4000 Hz. Figure 6 shows the frequency spectrum at different monitor pints. It is found that the peak value for different monitor points is observed at the frequency of 218 Hz which is the fundamental frequency of rotating rotor because its rotational speed is 6500 RPM. From the curve for the monitor point on the centerline, results show that the amplitude fluctuates between -10dB to 20dB and does not change a lot with frequency. However, the amplitude of the acoustic pressure for the monitor point at the lateral line decreases with the increase of the frequency from 0 Hz to 1500 Hz. The same tendency can be found for the monitor point at the blade tip. The amplitude changes dramatically with the frequency be-

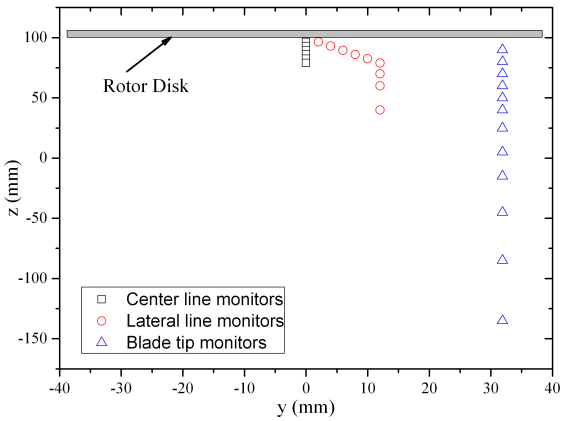

(a) Monitor point location

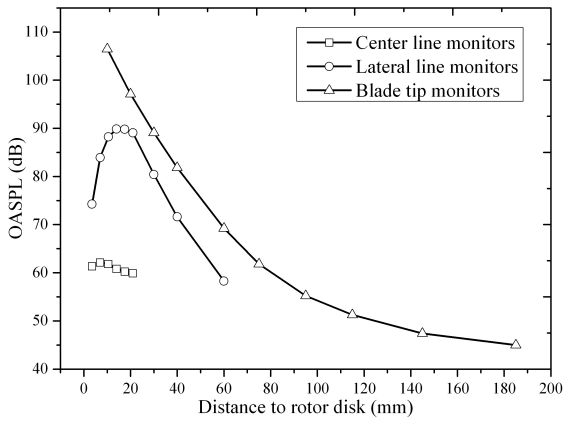

(b) OASPL varying with distance to rotor disk

Figure 4: Total sound pressure level in the wake.

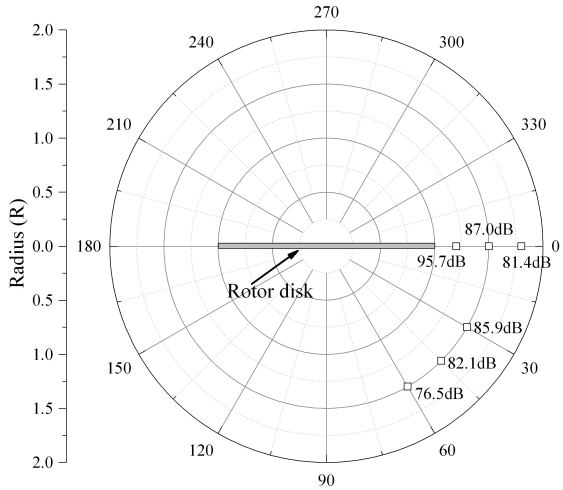

Figure 5: Total sound pressure level at different radius and angle.

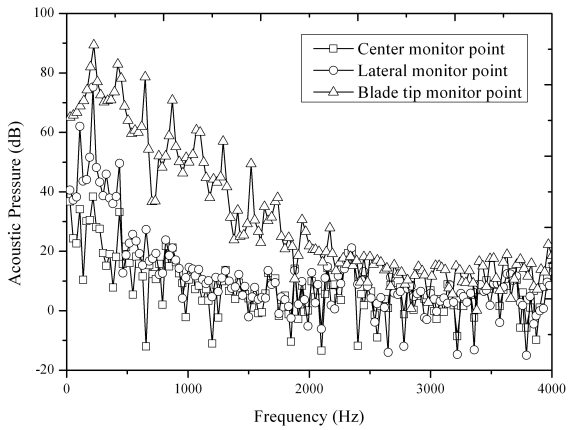

Figure 6: Frequency spectrum of aeronautics of shedding vortex.

fore 2000 Hz. The energy of the noise for single rotor mainly locates in the frequency lower than 2000 Hz. In summary, the aeroacoustic noise of nano rotor is mainly composed of the source related to blade thickness and the source linked to the aerodynamic loading. The peak value of the frequency spectrum curve has relation to shedding vortex and the maximum value is achieved at the fundamental frequency of the rotation. The aeroacoustic sources are surface source. The OASPL decreases with the increase of the distance to rotor disk.

To validate the computational method, the experiments were carried out with the aeroacoustics test bench for single rotor. Figure 7 shows the frequency spectrum of aeronautics at the distance of 20 mm to the blade tip in the wake for both experiment and computation. The frequency spectrum of aeronautics shows the typical characteristics of frequency spectrum for rotational rotor. The maximum peak amplitude locates at the frequency of 226 Hz which close to the fundamental frequency of 218 Hz. It is due to the error of the rotational velocity of the motor. At the frequency multiplication, peak values can be obtained which is due to the shedding of the vortex. When comparing with computational results, more smaller peak values are found. It is caused by the fabrication error of the rotor resulting in the asymmetry of the two blades. At the low frequency the difference between the experiment results and computational results is small, but it is high at high frequency. Figure 8 shows that the OASPL at different monitor points on rotor disk. Results show that the computational results match well with experimental results. In summary, the computational method can predict the aeroacoustics characteristics of nano rotor well.

3.2 *Aeroacoustics Characteristics of Nano Coaxial Rotor*

The distance between upper rotor and lower rotor is 40 mm. The meshes were generated for nano coaxial rotor. The basic parameters of the meshes and the computational method are same to that for single upper rotor. The simulations were

IMAV2017-7
https://www.imavs.org/pdf/imav.2017.7

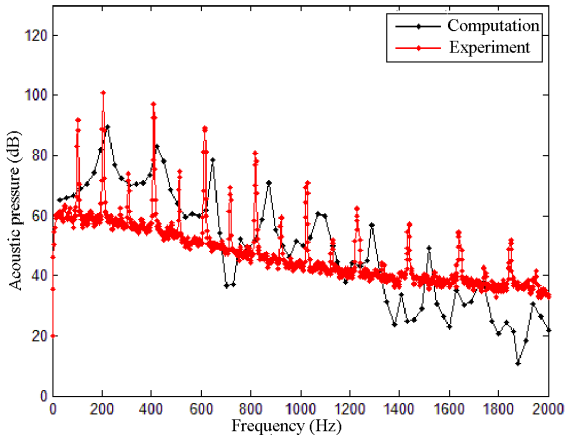

Figure 7: Frequency spectrum of aeronautics at the distance of 20 mm to the blade tip in the wake.

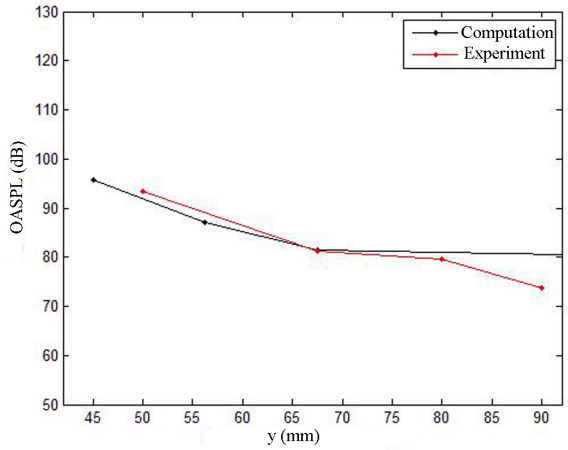

Figure 8: Comparison of OASPL for experiment and computation.

carried out on the both rotors at a tip Mach of 0.075. The rotor rotated 1 degree at each physical time step. Rotors rotated more than 10 cycles.

Figure 9 shows the vorticity magnitude contour at the section of $y = 0$ of the flow field for nano coaxial rotor. The figure illustrates that more vortices are generated between the lower rotor and the upper rotor besides the tip vortex. The strength of the shedding vortex in the wake of the lower rotor is higher than that of the single upper rotor. The vortices in the wake of the upper rotor are stretched due to the interaction of the lower rotor. And the tip vortices of the upper rotor are attract into the upstream flow of the lower rotor. The flow field of the nano coaxial rotor is more complicate than the single upper rotor.

The total sound pressure level was calculated for nano coaxial rotor. Figure 10(a) shows the monitor points in aeroa-

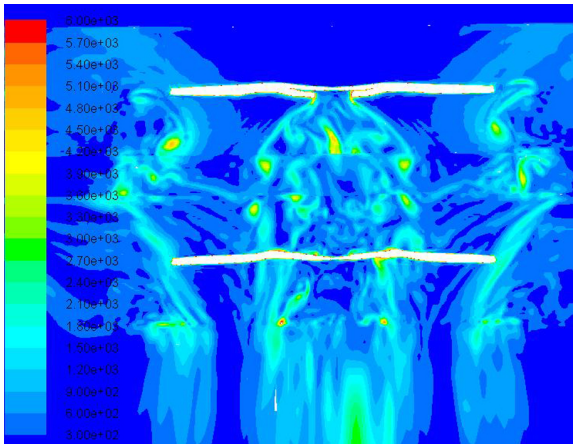

Figure 9: Vorticity magnitude contour of the $y = 0$ section for nano coaxial rotor.

coustic field for nano coaxial rotor. Three types of monitor points were generated as the case for single upper rotor. When comparing the OASPL for single rotor and the coaxial rotor, it is found that the OASPL at the monitor point on the center line for coaxial rotor is higher than that for single rotor as illustrated in Figure 10(b). But for the monitor points on the lateral line and blade tip, one can find that the OASPL for coaxial rotor is lower than that for single rotor when the monitor points locate between the two rotors. But it is far higher than that for single rotor when the monitor points locate below the lower rotor. Results indicates that the interference between upper rotor and lower rotor decreases the total sound pressure level for upper rotor but enhances the total sound pressure level for lower rotor. The total sound pressure level at different radius and angles in vertical plane was calculated. Two radii of 1.5 R and 2.0 Rand four angles of 0°, 30° and 45° were chosen to set monitor points as illustrated in Figure 11(a). From Figure 11(b), results show that the OASPL increases with the increase of the angle for both radii of 1.5 R and 2.0 R for the nano coaxial rotor. But the OASPL decreases with the increase of the angle for single rotor. And the OASPL for coaxial rotor is higher than that for single rotor. From 11(a), it can be found that the monitor points get close to the lower rotor with the increase of angle for nano coaxial rotor, which is consider as the reason. The interaction between rotors enhances the OASPL as well.

4 Conclusion

The interference between rotors on aeroacoustics was investigated for nano coaxial counter-rotating rotor. The aeroacoustics characteristics of single upper rotor were firstly studied with transient 3D LES CFD method coupling with FW-H method. And the experiments were carried out to validate the computational method. The total sound pressure level and the frequency noise spectrum of the upper rotor were moni-

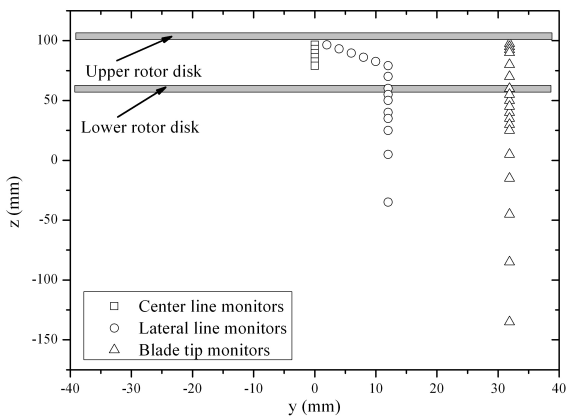

(a) Monitor point location

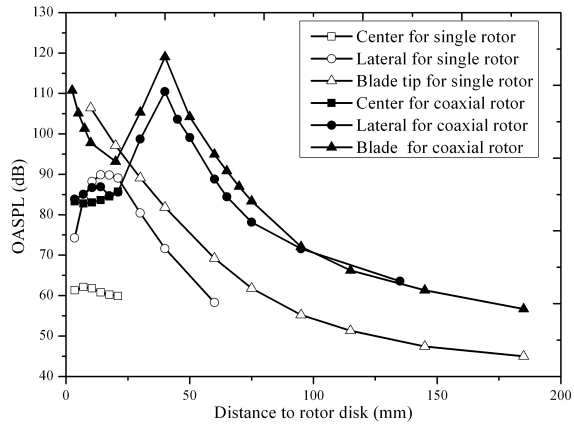

(b) OASPL varying with distance to rotor disk

Figure 10: Total sound pressure level in the wake for nano coaxial rotor.

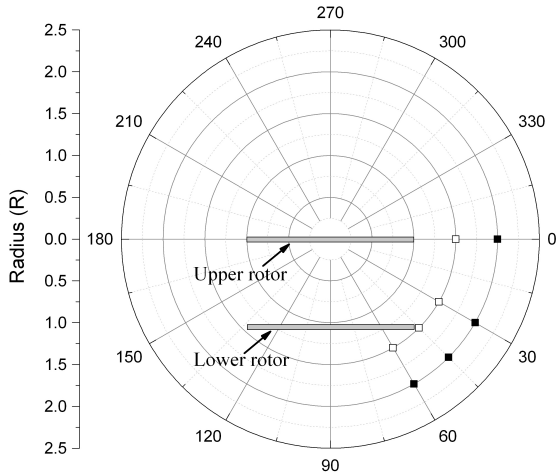

(a) Monitor point location

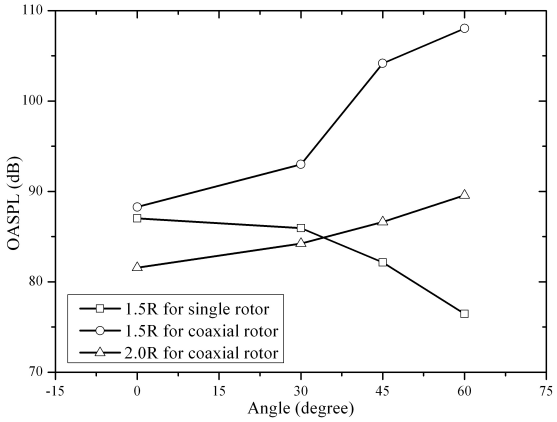

(b) OASPL varying with angle and radius

Figure 11: Total sound pressure level varying with the angle and radius.

tored. It is found that the total sound pressure level achieved its maximum value at blade tip. It is considered that the blade tip vortex is one important source for aeroacoustics of rotor. In the frequency noise spectrum, there is an integer in multiple of the rotation frequency and fundamental frequency, and the peak value decreases with the increase of frequency. The experimental aeroacoustics results match well with that of the computational results so that the computational method is validated. The aeroacoustics of nano coaxial rotor was then studied numerically. When comparing with upper rotor, it was found that the SPL of nano coaxial rotor increased. Flow field analysis showed that the shedding vortices of upper rotor interact the lower rotor resulting the blade-vortex interaction. It is evident that the aeroacoustics was enhanced by the interference of upper rotor and lower rotor.

Acknowledgements

The authors would like to thank the support of the National Natural Science Foundation of China (Grant No. 11302164), the Specialized Research Fund for the Doctoral Program of Higher Education of China (20130201120031), and the Fundamental Research Funds for the Central Universities (Grant No. xjj2013031).

References

[1] D.J. Pines. 06-06 proposer information pamphlet (pi) for defense advanced research project agency (darpa) defense sciences office (dso) nano air vehicle (nav) program. In *DARPA DSO*, 2005.

[2] Z. Liu, A. Roberto, J.M. Moschetta, and C. Thipyopas. Experimental and computational evaluation of small micro coaxial rotor in hover. *Journal of Aircraft*, 48(220-229), 1 2011.

[3] S. Sato, M.Drela, J.H. Lang, and D.M. Otten. Design and characterization of hover nano air vehicle propul-

IMAV2017-7
https://www.imavs.org/pdf/imav.2017.7

sion system. In *27th AIAA Applied Aerodynamics Conference*, 2009.

[4] H. Youngren, C. Kroninger, M. Chang, and S. Jameson. Low reynolds number testing of the ag38 airfoil for the samarai nano air vehicle. In *46th AIAA Aerospace Sciences Meeting and Exhibit*, 2008.

[5] M.M. Logue and H.M. Atassi. Modeling broadband rotor interaction noise. In *17th AIAA/CEAS Aeroacoustics Conference (32nd AIAA Aeroacoustics Conference)*, 2011.

[6] F. Farassat and M. K. Myers. Extension of kirchhoff's formulation to radiation from moving surface. *Journal of Sound and Vibration*, 123(3):451–460, 1988.

[7] J.E. Ffowcs Williams and D.L. Hawkings. Sound generated by turbulence and surfaces in arbitrary motion. *Philosophical Transactions of the Royal Society*, A264(1151):321–342, 1969.

[8] F. Farassat. Linear acoustic formulas for calculation of rotating blade noise. *AIAA Journal*, 19(9):1122–1130, 1981.

[9] G. Sinibaldi and L. Marino. Experimental analysis on the noise of propellers for small uav. *Applied Acoustics*, 74(1):79–88, 2013.

[10] L. Marino. Experimental analysis of uav-propellers noise. In *16th AIAA/CEAS Aeroacoustics Conference*, 2010.

[11] J.A. Housman and C.C. Kiris. Structured overlapping grid simulations of contra-rotating open rotor noise. In *AIAA 54th Aerospace Sciences Meeting*, 2016.

[12] S. Yi, H. Kwon, D. Im, S. Choi, and D. Lee. Noise characteristics of contra-rotating open rotor with time-spectral cfd and aeroacoustics analysis. In *54th AIAA Aerospace Sciences Meeting*, 2016.